

## Notes on the creation and manipulation of solid solution models

Robert Myhill · James Connolly

Received: date / Accepted: date

**Abstract** A large class of solid solution models are built on the premise that exchange of chemical species takes place on a finite number of unique sites, and that the thermodynamic properties of the solution are a function of the proportions of species occupying each of the sites. The site-occupancy spaces spanned by such models are geometrically equivalent to convex polytopes,  $n$ -dimensional generalisations of polygons and polyhedra. The endmembers of these solid solutions correspond to the vertices of the polytopes.

We present a set of mathematical tools based on this geometrical equivalence which aid the creation and manipulation of solution models. Vertex enumeration methods can be used to compute the total set of endmembers in a solution from the valences of the species occupying each site and the total charge of the species not involved in site exchange. The number of independent endmembers constructed in this way is equal to  $n_{site-species} - n_{sites} + c$ , where  $n_{site-species}$  is the total number of potential site-species occupancies in the solution and  $n_{sites}$  is the number of distinct sites. If charge-balance constraints are active,  $c = 0$ , otherwise  $c = 1$ .

We also present the linear algebra required to transform solution model parameterisations between different independent endmember bases. The same algorithms can also be used to derive macroscopic endmember interactions from microscopic site interactions. This algebra is useful both in the initial design of solution models, and when making thermodynamic calculations in restricted chemical subsystems.

---

R. Myhill  
School of Earth Sciences, University of Bristol. Wills Memorial Building, Queen's Road,  
Bristol BS8 1RJ  
E-mail: bob.myhill@bristol.ac.uk

J.A.D. Connolly  
Institut für Mineralogie und Petrographie ETH-Zentrum, Clausiusstrasse 25. CH-8092,  
Zürich, Switzerland

A polytope description of solid solutions is now used in the thermodynamic software *PerpleX* and *burnman*. The algorithms described here are made available as python code.

**Keywords** solid · solution · creation · manipulation

## 1 Introduction

Solid solution models are an essential component in modelling geological, metallurgical and other chemical processes. The motivation behind this paper is to introduce some mathematical background defining the structure and properties of commonly used solution models, and to introduce tools that aid in their construction and manipulation. We concentrate on solution models which have a constant number of sites per formula unit, and where interactions are dependent only on the total proportions of species occupying each site. We do not consider models which explicitly involve local interactions, such as bonding between pairs or clusters of species [1,2].

## 2 An algebraic description of solid solutions

### 2.1 Solid solutions as polytopes

Substitutional solid solutions can be written in the form:

$$[A, B]_y^Y [B, C, D]_z^Z \dots \quad (1)$$

where the square brackets denote distinct sites in the structure, and the comma-separated lists are the species that can occupy each site. In the example above, species A and B can occupy Site Y, which has a multiplicity of  $y$  per formula unit, and species B, C and D can occupy Site Z, which has a multiplicity of  $z$ . Throughout this paper, the species which can occupy each site for any given solution are called *site-species*. There are five site-species in Equation 1:  $A^Y$ ,  $B^Y$ ,  $B^Z$ ,  $C^Z$  and  $D^Z$  ( $n_{\text{site-species}} = 5$ ).

We define the site-occupancy space of any solid solution as the set of site-species occupancies which satisfy the chemical formula of the solution. This space is mathematically equivalent to a convex polytope (the  $n$ -dimensional equivalent of a polyhedron). That is, the set  $\mathcal{X}$  of valid site-species occupancies  $\mathbf{x}$  of a solid solution can be described using an  $m \times n_{\text{site-species}}$  matrix  $\mathbf{P}$  and a vector  $\mathbf{b}$  of length  $m$ :

$$\mathcal{X} = \{\mathbf{x}; \mathbf{P}\mathbf{x} = \mathbf{b}; x_i \geq 0\} \quad (2)$$

where  $m$  is the number of independent constraints on the site populations. For solutions where each site can be occupied only by species with equal charges,  $m$  is equal to the number of sites. In this case, each row of  $\mathbf{P}$  corresponds to a distinct site (such as the dodecahedral site in garnet), and each column to a site-species (such as Mg on the dodecahedral site). Each component of  $\mathbf{P}$

is equal to zero unless the column and row correspond to the same site, in which case the component is equal to one. The components of  $\mathbf{b}$  are all equal to one. Charge-balance can be incorporated as an additional row in matrix  $\mathbf{P}$  and component in vector  $\mathbf{b}$ , with the new components of  $\mathbf{P}$  corresponding to the charges of each site-species multiplied by the site multiplicity, and the new value in  $\mathbf{b}$  corresponding to the total charge over all the sites.

We illustrate this formalism by way of a few examples (Figure 1). Single-site solutions where all site-species have the same valence can be represented by a matrix  $\mathbf{P}$  equal to a  $1 \times n_{\text{site-species}}$  vector of ones, and a vector  $\mathbf{b}=1$ . The resulting constraints on the site populations can be written as

$$\sum_{i=1}^{n_{\text{site-species}}} x_i = 1 \quad (3)$$

These solutions can be represented graphically as  $(k-1)$ -simplexes, the  $(k-1)$ -dimensional equivalent of a triangle (Figure 1a and b).

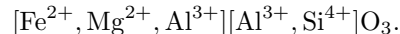
Single site solutions can also involve site-species with more than one charge. One example is pyrope-majorite garnet. At extremely high temperatures ( $>3000$  K), this solution can be reasonably approximated as  $\text{Mg}_3[\text{Mg}, \text{Al}, \text{Si}]_2\text{Si}_3\text{O}_{12}$ , with mixing of Mg, Al and Si on a single octahedral site [3]. The corresponding polytope matrix and vector for this solution are provided (Table 1). The

**Table 1** Polytope matrix  $\mathbf{P}$  and vector  $\mathbf{b}$  for a one-site pyrope-majorite garnet.

	Site Y (multiplicity 2)			b
	Mg <sup>2+</sup>	Al <sup>3+</sup>	Si <sup>4+</sup>	
Y-site	1	1	1	1
Charge-balance	4	6	8	12

charge-balance constraint in Table 1 can be represented graphically by a line cutting through the original 2-simplex (Figure 1c). The two endpoints of this line correspond to the endmembers pyrope ( $\text{Mg}_3[\text{Al}]_2\text{Si}_3\text{O}_{12}$ ) and disordered majorite ( $\text{Mg}_3[\text{Mg}_{0.5}\text{Si}_{0.5}]_2\text{Si}_3\text{O}_{12}$ ).

We now turn to multi-site solutions. The site-occupancy space of multi-site solutions cannot be represented by simplices, but rather by the Cartesian product of the individual site-simplices. If a charge-balance constraint is involved, the site-occupancy space is restricted to the intersection of the raw Cartesian product with a hyperplane. We illustrate this general case with a two-site bridgmanite in the simple system  $\text{FeO}-\text{MgO}-\text{Al}_2\text{O}_3-\text{SiO}_2$ , whose general formula can be expressed as



The matrix  $\mathbf{P}$  and vector  $\mathbf{b}$  for the polytope corresponding to this solution have three rows; one for each site and one for the charge-balance constraint (Table 2). Each vertex of this polytope corresponds to an ordered endmember in the solid solution (Figure 1d):  $\{[\text{Mg}][\text{Si}], [\text{Fe}][\text{Si}], [\text{Al}][\text{Al}]\}$ . Here we define an

ordered endmember as any instance of a solid solution where each site is occupied by a single species (i.e. where the solution has a configurational entropy of zero). This differs from other studies, which define ordered compounds as those where multi-site species reside on only a subset of their potential sites [4,5].

**Table 2** Polytope matrix  $\mathbf{P}$  and vector  $\mathbf{b}$  for a two-site FMAS bridgmanite including full order-disorder.

	Site A			Site B		b
	Fe <sup>2+</sup>	Mg <sup>2+</sup>	Al <sup>3+</sup>	Al <sup>3+</sup>	Si <sup>4+</sup>	
A-site	1	1	1	0	0	1
B-site	0	0	0	1	1	1
Charge-balance	2	2	3	3	4	6

Finally, a three-site solution whose site-occupancy space can be represented in three dimensions is [Cu, Ag]<sub>10</sub>[Fe, Zn]<sub>2</sub>[Sb, As]<sub>4</sub>S<sub>13</sub> fahlore [6] (Figure 1e). Most solution models have no simple representation in three dimensions, but the examples in Figure 1 provide the insights necessary to understand site-occupancy spaces of arbitrary complexity.

## 2.2 Endmember enumeration

For simple solutions, the full set of endmembers are easily enumerated by hand. However, for complex solutions, this task is significantly more arduous. By expressing a solid solution in polytope form (Equation 2), standard vertex enumeration algorithms can be used to find all the endmembers [7, 8, 9]. These algorithms yield an endmember site-occupancy matrix  $\mathbf{E}$ , where each component  $E_{ij}$  comprises the fractional occupancy of site-species  $j$  in a distinct endmember  $i$ . The resulting number of endmembers may be much larger than the number of site-species. For solid solutions with no charge-balance constraints, the number of endmember vertices grows geometrically with the number of sites:

$$n_{mbrs} = \prod_{i=1}^{n_{sites}} n_{species,i} \quad (4)$$

where  $n_{species,i}$  is the number of species on site  $i$ . Despite the geometric growth in the **total** number of endmembers, the number of **independent** endmembers grows linearly with the number of sites. A potential set of independent endmembers can be computed in several ways, including as a by-product of finding the row-reduced en-echelon form of  $\mathbf{E}$ . One such implementation is found in the algorithms linked in the Appendix. Taking the dot product of the transpose of  $\mathbf{E}^{ind}$  with a vector of independent endmember proportions  $\mathbf{p}^{ind}$  yields the site-species occupancies  $\mathbf{x}$  of any instance of a solution:

$$E_{ji}^{ind} p_j^{ind} = x_i \quad (5)$$

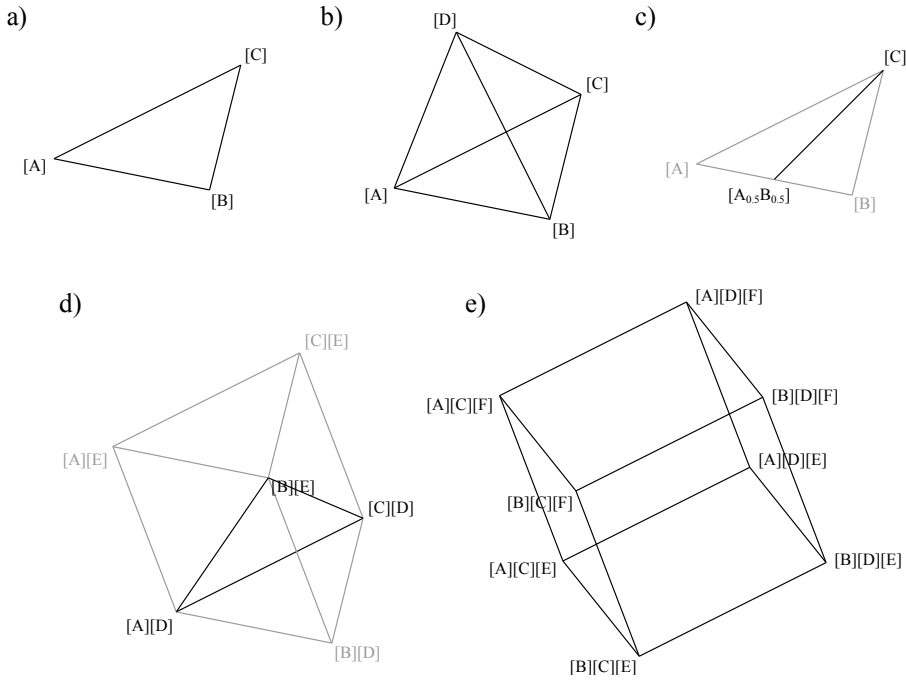


**Fig. 1** Polytopes corresponding to some 1-site (a-c), 2-site (d) and 3-site (e) solution models. The dimensionality of an  $n$ -site solution model without charge-balance constraints is equal to  $\sum_{i=1}^n (k_i - 1)$ , where  $k_i$  is the number of endmembers on site  $i$ , restricting the variety of polytopes which can be represented graphically in 3-dimensions. a) A 2-simplex, such as  $[\text{Mg}, \text{Fe}, \text{Ca}]_3\text{Al}_2\text{Si}_3\text{O}_{12}$  garnet. b) A 3-simplex, such as  $[\text{Mg}, \text{Fe}, \text{Ca}, \text{Mn}]_3\text{Al}_2\text{Si}_3\text{O}_{12}$  garnet. c) A subset of a 2-simplex, such as a one-site pyrope-majorite solution  $\text{Mg}_3[\text{Mg}, \text{Al}, \text{Si}]_2\text{Si}_3\text{O}_{12}$ , where a charge-balance constraint limits the valid site-occupancy space (see Table 1). Grey lines mark the original 2-simplex without charge-balance constraints. d) A subset of the Cartesian product of a 3-simplex and 2-simplex, such as  $[\text{Fe}, \text{Mg}, \text{Al}][\text{Al}, \text{Si}]\text{O}_3$ -bridgmanite (Table 2). Grey lines mark the original polytope without charge-balance constraints. e) The Cartesian product of three 2-simplexes, e.g.  $[\text{Cu}, \text{Ag}]_{10}[\text{Fe}, \text{Zn}]_2[\text{Sb}, \text{As}]_4\text{S}_{13}$  fahlore [6].

### 2.3 Constructing a polytope from an existing set of independent endmembers

The previous section described how to compute a complete set of endmembers and an independent endmember basis from a set of known site-species and their valences. This is a fundamental first-step for anyone wishing to construct a solution model, and can be a time-consuming and error-prone task to compute by hand. The following section describes the inverse procedure: how a set of independent endmembers can be used to construct the polytope matrix  $\mathbf{P}$  and vector  $\mathbf{b}$ .

First, we populate the independent endmember site-occupancy matrix  $\mathbf{E}^{ind}$ . Table 3 shows the elements of  $\mathbf{E}^{ind}$  for the two-site bridgmanite described in Section 2.1. A polytope matrix  $\mathbf{P}$  and vector  $\mathbf{b}$  of this solution can be computed from the right nullspace (or kernel) of  $\mathbf{E}^{ind}$ , defined as a set of independent

**Table 3** The independent endmember site-occupancy matrix  $\mathbf{E}^{ind}$  for a two-site FMAS bridgmanite including full order-disorder.

Endmember	Site A			Site B	
	Fe <sup>2+</sup>	Mg <sup>2+</sup>	Al <sup>3+</sup>	Al <sup>3+</sup>	Si <sup>4+</sup>
[Fe][Si]O <sub>3</sub>	1	0	0	0	1
[Mg][Si]O <sub>3</sub>	0	1	0	0	1
[Al][Al]O <sub>3</sub>	0	0	1	1	0

site-species occupancy vectors  $\mathbf{x}$  which satisfy the expression:

$$\mathcal{N}(\mathbf{E}^{ind}) = \{\mathbf{x}; \mathbf{E}^{ind}\mathbf{x} = \mathbf{0}\} \quad (6)$$

Note that Equations 2 and 6 are both sets based on a set of linear equalities involving the site-species occupancy vectors. Indeed, the sets can be made identical by adding to Equation 6 the requirement that the sum of the site-species occupancy fractions equals the number of sites. Therefore, a polytope matrix  $\mathbf{P}$  can be constructed by adding a row of ones to the right nullspace of  $\mathbf{E}^{ind}$ , and the vector  $\mathbf{b}$  can be constructed from the null vector  $\mathbf{0}$  by appending a component with value equal to the number of sites in the solution.

This construction reveals a relationship between the shape of  $\mathbf{E}^{ind}$  and the number of constraints  $m$  defining the polytope. As the  $n_{ind-mbrs} \times n_{site-species}$  matrix  $\mathbf{E}^{ind}$  is, by-definition, of full row-rank, the dimension of  $\mathcal{N}(\mathbf{E}^{ind})$ , its nullity, must be equal to  $n_{site-species} - n_{ind-mbrs}$ . As  $\mathbf{P}$  can be constructed by adding a single row to  $\mathcal{N}(\mathbf{E}^{ind})$ , it follows that

$$\begin{aligned} m &= \text{rank}(\mathbf{P}) \\ &= \text{nullity}(\mathbf{E}^{ind}) + 1 \\ &= n_{site-species} - n_{ind-mbrs} + 1 \end{aligned} \quad (7)$$

From Section 2.1,  $m$  is equal to the number of sites, plus one if charge-balance needs to be considered. Thus, the number of independent endmembers describing the full site-occupancy space of any solid solution is governed by the relationship:

$$n_{ind-mbrs} = n_{site-species} - n_{sites} + c \quad (8)$$

where  $c = 0$  if charge-balance needs to be considered, and  $c = 1$  otherwise.

#### 2.4 Subspaces and degeneracy within solid solutions

If no single species can exist on more than one site, like in the [Cu, Ag]<sub>10</sub>[Fe, Zn]<sub>2</sub>[Sb, As]<sub>4</sub>S<sub>13</sub> fahlore solution [6], every point in site-occupancy space defines a unique bulk composition of the solution and the composition space of the solution is therefore identical to its site-occupancy space. Such solutions are known as reciprocal solutions. Non-reciprocal solutions host two or more species which mix across sites (e.g. Mg and Fe in [Mg, Fe][Mg, Fe]Si<sub>2</sub>O<sub>6</sub>-pyroxene). In these

solutions, referred to as order-disorder solutions, the composition and site-occupancy spaces are not equivalent.

The shape of a polytope spanning the site-occupancy space of a solid solution does not depend on whether a solution model is reciprocal or not. It depends only on the number of sites, and the number and total charge of site-species on those sites. Polytopes for a reciprocal solution with different species on all sites ( $[A,B][C,D][E,F]$ ) and a non-reciprocal solution where the same species appear on all three sites ( $[A,B][A,B][A,B]$ ) will therefore have the same shape (Figure 2).

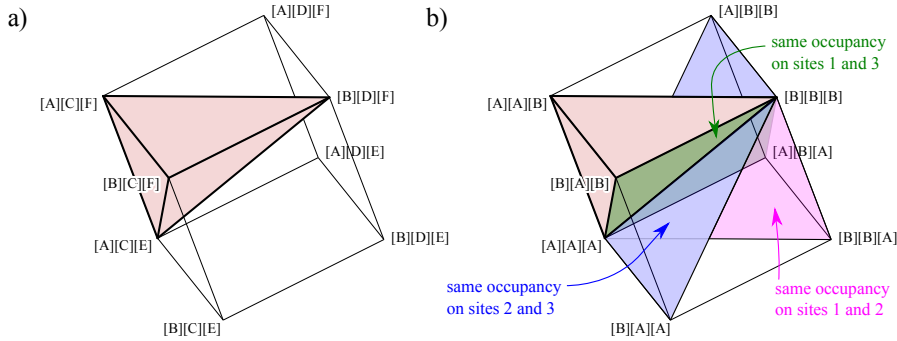


**Fig. 2** Polytopes for two different three-site solutions. a) A polytope representing a solution where the three sites “[...]” are occupied by different species, denoted A–F:  $[A,B][C,D][E,F]$ . The shaded tetrahedron shows a subspace of the solution whose vertices represent one potential set of independent endmembers. b) A polytope representing a solution where the three sites are now filled with similar components:  $[A,B][A,B][A,B]$ . Coloured planes mark where two sites have the same proportions of A and B. Again, the shaded tetrahedron shows the subspace of the solution whose vertices represent one potential set of independent endmembers.

For the reciprocal solution (Figure 2a), every point within the polytope has a unique composition. In contrast, the compositional space of the order-disorder solution (Figure 2b) is one-dimensional. Planes perpendicular to AAA–BBB represent instances of the solid solution with exactly the same bulk composition, but different distributions of species A and B amongst the three sites. The vertices of the tetrahedra in Figure 2 represent one potential set of independent endmembers. A linear combination of these endmembers is sufficient to describe any site-occupancy within the solution; if the site-occupancy lies outside the tetrahedron, one or more proportions will be negative.

Up to this point, we have restricted ourselves to discussing the site occupancy space of solutions without reference to the energetics of mixing or the most energetically stable arrangement of species within solutions of fixed composition. A review of the various formulations for the energetics of solid solutions is beyond the scope of this paper, but it is worth noting that within solutions capable of undergoing order-disorder, (a)symmetries in the energy landscape within the occupancy space of the solution may dictate which parts

of the solution can be stable. For the order-disorder solution  $[A,B][A,B][A,B]$  (Figure 2b):

- If there is no energetic preference for A and B to reside on different sites, all stable points will lie along AAA–BBB, i.e., the solution will be fully disordered at all temperatures.
- If all three sites are identical with respect to A,B occupancy and interaction energies (see Section 3.2), a single tetrahedron contains all the relevant thermodynamics of the system; the energy landscape of the other tetrahedra can be calculated by reflecting the landscape of the first tetrahedra in the planes shown in Figure 2b. Such solutions will become completely disordered at high temperatures, but are not necessarily disordered at low temperatures.
- If the energies associated with A,B occupancy and exchange are not identical for all three sites, one or more tetrahedra may only be energetically stable under particular pressure-temperature-composition conditions, or may be metastable under all conditions. In other words, the solution will remain partially ordered at all temperatures.

We illustrate these three cases for a two-site solution model  $[A,B][A,B]$  (Figure 3). In Figure 3a, A-B exchange on the same site is associated with an interaction energy of 1 kJ/mol, while the cross-site reaction  $[A][A] + [B][B] \longrightarrow 2[A][B]$  is 4 kJ/mol, favouring disorder. In Figure 3b, the energy of the cross site reaction is reduced to -4 kJ/mol, favouring ordering at low temperatures. Note the symmetry about the line of complete disorder in Figures 3a and b. At high temperatures, the contribution of the configurational entropy to the Gibbs free energy (Figure 3d) will lead to complete disorder at all compositions. Finally, in Figure 3c, the energy associated with A residing on Site 1 is raised by 1 kJ/mol. The symmetry of the previous two cases is now broken. Under this circumstance, the portion of site-occupancy space in the upper-left hand triangle will always be thermodynamically unstable. The degree of disorder will still increase with increasing temperature, but instances of this solution will always remain partially ordered.

## 2.5 Identifying and avoiding “logical inconsistencies” in solution models

If a solid solution model has fewer independent endmembers than that suggested by Equation 8, then the model includes at least one constraint which is not related to charge-balance. Sometimes, these choices are made consciously, with the aim of reducing the number of endmembers or to avoid dealing with order parameters. However, the approximations implicit in these simplifications are not always reasonable.

We illustrate the problem using a two-site pyrope-majorite solution (Table 4), extending the one-site solution introduced in Section 2.1. This two-site solution allows for Mg and Si to reside on different sites. The site-occupancy space of this solution is a polytope with five endmember vertices, of which

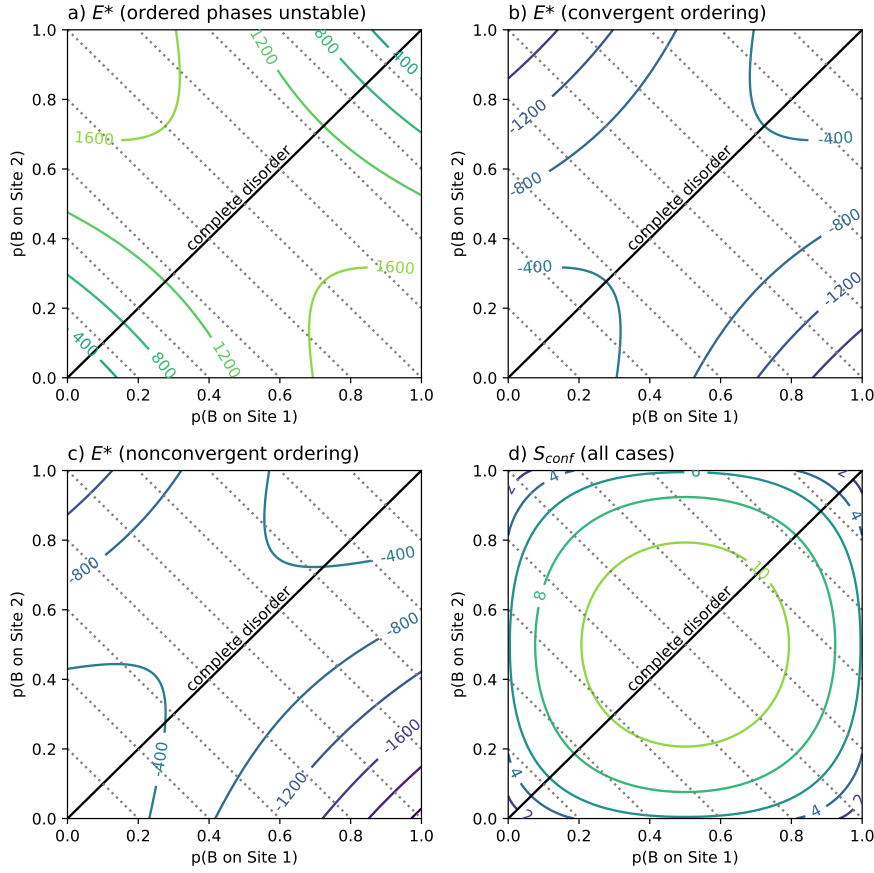


**Fig. 3** Excess non-configurational energy ( $E^*$ , J/mol) and configurational entropy ( $S_{conf}$ , J/K/mol) for a two-site, two-species order-disorder solution ( $[A,B][A,B]$ ) modelled with three different regular/symmetric solution models. Dotted lines represent lines of constant composition. The black line represents equal amounts of A and B on both sites. a) The ordered phases  $[A][B]$  and  $[B][A]$  are destabilised by a large positive energy of ordering. Both sites have identical properties. b) The ordered phases are stabilised at low temperatures. Both sites have identical properties. c) The ordered phases are again stabilised at low temperatures, but the two sites are now distinct, with an increased energy associated with A occupying Site 1. As a result, species B will always favour Site 1. d) Configurational entropy for all cases. See main text for further description.

**Table 4** Polytope matrix  $\mathbf{P}$  and vector  $\mathbf{b}$  for a two-site pyrope-majorite garnet.

	Site $Y_1$ (multiplicity 1)			Site $Y_2$ (multiplicity 1)			b
	Mg <sup>2+</sup>	Al <sup>3+</sup>	Si <sup>4+</sup>	Mg <sup>2+</sup>	Al <sup>3+</sup>	Si <sup>4+</sup>	
Y <sub>1</sub> -site	1	1	1	0	0	0	1
Y <sub>2</sub> -site	0	0	0	1	1	1	1
Charge-balance	2	3	4	2	3	4	12

any four are linearly independent. A possible set of independent endmembers is  $\{[\text{Mg}][\text{Si}], [\text{Si}][\text{Mg}], [\text{Al}][\text{Al}], [\text{Al}][\text{Mg}_{0.5}\text{Si}_{0.5}]\}$ , with the dependent endmember in this case being  $[\text{Mg}_{0.5}\text{Si}_{0.5}][\text{Al}]$ . Splitting the sites has not removed all disordered endmembers. Depending on the choice of endmember and interaction energies, it may be that this disordered endmember never contributes to the free energy of the stable compound. However, there is no guarantee that this will always be the case, especially if energies are defined based on an analysis of atomic-interactions (Section 3.2), see also [10]. There are many examples where reducing the number of independent endmembers is unreasonable. Holland and Powell [5] used the example of Mg-Fe-Al orthopyroxene  $[\text{Mg}, \text{Fe}, \text{Al}][\text{Mg}, \text{Fe}](\text{Al}, \text{Si})_2\text{O}_6$  (where mixing on the tetrahedral site is not treated explicitly), and showed that reducing the number of independent endmembers by splitting the Mg and Fe equally between the two sites was thermodynamically implausible.

Clinoamphibole provides a more complex example. One recent model includes 18 potential site-species distributed over six sites [11,12]. Using Equation 8, a complete model in this system should have 12 independent endmembers (Table 5, computed using freely available python code, see Appendix). The published model in this system has only 11 independent endmembers, and so does not span the full site-occupancy space of the solution. For such complex models, Equation 8 provides a vital consistency check.

**Table 5** Independent endmember site-occupancy matrix  $\mathbf{E}^{ind}$  for a six-site clinoamphibole solution model including full order-disorder. Site multiplicities are given in brackets. The *famph* endmember is one of many potential endmembers that completes the published endmember basis [11,12]. This solution model has a total of 432 endmembers.

name	A (1)			M <sub>13</sub> (3)		M <sub>2</sub> (2)			Fe <sup>3+</sup>	Ti	M <sub>4</sub> (2)			T (4)		V (2)		
	v	Na	K	Mg	Fe	Mg	Fe	Al			Ca	Mg	Fe	Na	Si	Al	OH	O
tr	1	0	0	1	0	1	0	0	0	0	1	0	0	0	1	0	1	0
ts	1	0	0	1	0	0	0	1	0	0	1	0	0	0	0.5	0.5	1	0
parg	0	1	0	1	0	0.5	0	0.5	0	0	1	0	0	0	0.5	0.5	1	0
gl	1	0	0	1	0	0	0	1	0	0	0	0	0	1	1	0	1	0
cumm	1	0	0	1	0	1	0	0	0	0	0	1	0	0	1	0	1	0
grun	1	0	0	0	1	0	1	0	0	0	0	0	1	0	1	0	1	0
a	1	0	0	1	0	0	1	0	0	0	0	0	1	0	1	0	1	0
b	1	0	0	0	1	1	0	0	0	0	0	0	1	0	1	0	1	0
mrbr	1	0	0	1	0	0	0	0	1	0	0	0	0	1	1	0	1	0
kprg	0	0	1	1	0	0.5	0	0.5	0	0	1	0	0	0	0.5	0.5	1	0
tts	1	0	0	1	0	0	0	0	0	1	1	0	0	0	0.5	0.5	0	1
famph	1	0	0	0	1	0	0	1	0	0	0	0	1	0	1	0	0	1

On the basis of this discussion, one may ask in which circumstances independent endmembers can be removed from a solution model. The following points should be borne in mind:

1. Independent endmembers should not be removed if they exclude regions of composition space in the chemical system of interest.
2. Endmembers which represent non-zero *and* non-maximal entropies at their given composition *may* be removed as long as they do not disobey Rule

- 1, with the understanding that their removal will render some of the full site-occupancy space inaccessible.
3. Once a full solution model has been constructed and parameterised, the extent of the accessible site-occupancy space under the conditions of interest can be determined. If the accessible space can be described by a smaller number of independent endmembers than the full site-occupancy space, then a modified polytope can be defined following the procedure in Section 2.3.

It should be stressed that simplifying solution models based on Rule 3 should not change the results of any thermodynamic calculations, and serves only to improve computational efficiency.

### 3 Manipulation of solid solution models

#### 3.1 Changing independent endmember bases

The previous section described how to consistently determine an independent endmember set for a solid solution, based on knowledge only of the number of distinct sites in the structure, and the potential species residing on each site. It also outlined potential pitfalls in attempts to simplify the resulting solution models. We now show how to convert endmember and interaction energies between sets (or bases) of independent endmembers. This conversion has two primary purposes:

- We often wish to solve thermodynamic problems in restricted compositional spaces. For example, we might want to model the almandine-skiagite binary in garnets ( $[\text{Fe}^{2+}]_3[\text{Fe}^{3+}, \text{Al}]_2\text{Si}_3\text{O}_{12}$ ) using a solution model where almandine ( $[\text{Fe}^{2+}]_3[\text{Al}]_2\text{Si}_3\text{O}_{12}$ ), grossular ( $[\text{Ca}]_3[\text{Al}]_2\text{Si}_3\text{O}_{12}$ ) and andradite ( $[\text{Ca}]_3[\text{Fe}^{3+}]_2\text{Si}_3\text{O}_{12}$ ) are the independent endmembers.
- We can use the same mathematics to convert interaction energies on the atomic scale (for example, the interaction between  $\text{Fe}^{2+}$  on one site and  $\text{Fe}^{3+}$  on another) into interactions between endmembers (for example, the interaction energy between almandine and andradite, see Section 3.2).

Throughout this section, the matrix  $\mathbf{A}$  is used to transform an independent endmember basis to a new basis. Each element of  $A_{ij}$  corresponds to the number of moles of original endmember  $i$  contained within the new endmember  $j$ . The proportions of the original endmember set  $p_i$  in terms of the new endmember set  $p'_i$  are thus given by:

$$p_i = A_{ij}p'_j \quad (9)$$

The following subsections outline the mathematics to convert endmember bases within the “asymmetric” [13] and “subregular” [14] mixing model formulations. “Ideal”, “symmetric/regular” solution models can be viewed as special cases of these more general formalisms.

### 3.1.1 The asymmetric model

Changing endmember basis for the asymmetric model has been described in Diener et al. [15]. It is included here both for completeness and to provide an alternative derivation using Einstein summation convention. Repeated indices are summed over unless they appear on both sides of the equation. The non-configurational Gibbs free energy is given as a function of the proportions of an independent set of endmembers  $p_i$ :

$$G^* = p_i G_i^{mbr} + \alpha_i p_i \alpha_j p_j W_{ij}^B / f \quad (10)$$

$$f = \alpha_k p_k \quad (11)$$

where  $G_i^{mbr}$  is the Gibbs free energy of endmember  $i$ ,  $\alpha_i$  is the van Laar (asymmetry) parameter for that endmember, the components of  $W_{ij}^B$  are equal to  $2W_{ij}/(\alpha_i + \alpha_j)$ , and  $\mathbf{W}$  is an upper triangular matrix containing the binary endmember interaction parameters. The endmember and interaction terms can be combined into a single combined matrix  $\mathbf{W}^C$ :

$$G^* = \alpha_i p_i \alpha_j p_j W_{ij}^C / f \quad (12)$$

$$W_{ij}^C = W_{ij}^B + ((G^{mbr}/\alpha)_i 1_j + 1_i (G^{mbr}/\alpha)_j) / 2 \quad (13)$$

Combining Equations 9 and 12 yields:

$$G^* = \alpha_i A_{il} p'_l \alpha_j A_{jm} p'_m W_{ij}^C / f \quad (14)$$

$$f = \alpha_k A_{kn} p'_n \quad (15)$$

In order to transform this new expression into the same form as Equation 10, we first define new asymmetry parameters  $\alpha'$  and matrices  $\mathbf{B}$  and  $\mathbf{C}$ :

$$\alpha'_l = \alpha_i A_{il} \quad (16)$$

$$B_{il} \alpha'_l = C_{il} = \alpha_i A_{il} \quad (17)$$

such that

$$B_{il} = \alpha_i A_{il} (1/\alpha'_l) \quad (18)$$

Substituting these expressions into Equation 15 yields

$$G^* = B_{il} \alpha'_l p'_l B_{jm} \alpha'_m p'_m W_{ij}^C / f' \quad (19)$$

$$f' = \alpha'_n p'_n \quad (20)$$

The interaction matrix can now be transformed to yield an expression in the form of Equation 10:

$$G^* = \alpha'_l p'_l \alpha'_m p'_m W'_{ij}{}^C / f' \quad (21)$$

$$W'_{lm}{}^C = B_{il} B_{jm} W_{ij}^C \quad (22)$$

The transformed endmember properties are now removed from  $\mathbf{W}'^C$ . This is the reverse of the operation in Equation 12:

$$G_l'^{mbr} = \alpha_l' W_{ll}'^C \quad (23)$$

$$D_{lm} = W_{lm}'^C - ((G_l'^{mbr}/\alpha_l')1_m + 1_l(G_m'^{mbr}/\alpha_m'))/2 \quad (24)$$

Finally, the binary can be converted back to upper triangular form by summing the upper and lower triangular components of  $\mathbf{D}$ :

$$W_{lm}'^B = \begin{cases} D_{lm} + D_{ml}, & \text{if } l < m \\ 0, & \text{otherwise} \end{cases} \quad (25)$$

where the components of  $W_{lm}'^B$  are equal to  $2W_{lm}'^C/(\alpha_l' + \alpha_m')$ .

### 3.1.2 The subregular model

In the subregular model, the non-configurational Gibbs free energy includes unary  $\mathbf{G}^{mbr}$ , binary  $\mathbf{W}^B$  and ternary  $\mathbf{W}^T$  contributions [14]:

$$G^* = p_i G_i^{mbr} + p_i p_j W_{ij}^B (1 + p_j - p_i)/2 + p_i p_j p_k W_{ijk}^T \quad (26)$$

This equation can be transformed into a single term involving a combined interaction matrix  $\mathbf{W}^C$ :

$$G^* = p_i p_j p_k W_{ijk}^C \quad (27)$$

where

$$W_{ijk}^C = (G_i^{mbr} 1_j 1_k + G_j^{mbr} 1_i 1_k + G_k^{mbr} 1_i 1_j)/3 + (1_i W_{jk}^B + W_{ij}^B I_{jk} - W_{ij}^B I_{ik})/2 + W_{ijk}^T \quad (28)$$

The transformed interaction matrix  $\mathbf{W}'^C$  is computed using the relationship between the original and transformed endmember proportions (Equation 9):

$$G^* = A_{il} p_l' A_{jm} p_m' A_{kn} p_n' W_{ijk}^C \quad (29)$$

$$W_{lmn}'^C = A_{il} A_{jm} A_{kn} W_{ijk}^C \quad (30)$$

To convert this back into the form of Equation 26, we first remove the transformed endmember excesses from  $\mathbf{W}'^C$ :

$$G_l'^{mbr} = W_{ll}'^C \quad (31)$$

$$B_{lmn} = W_{lmn}'^C - (G_l'^{mbr} 1_m 1_n + 1_l G_m'^{mbr} 1_n + 1_l 1_m G_n'^{mbr})/3 \quad (32)$$

The transformed binary matrix  $\mathbf{W}'^B$  is then given by

$$W_{lm}'^B = (B_{lmn} + B_{mln} + B_{mnl}) I_{mn} \quad (33)$$

Removing  $\mathbf{W}'^B$  from  $\mathbf{B}$  leaves us with matrix  $\mathbf{C}$ :

$$C_{lmn} = B_{lmn} - 1_l W_{mn}'^B/2 \quad (34)$$

The transformed ternary components  $\mathbf{W}'^T$  can then be found by summing the six contributing terms in  $\mathbf{C}$ :

$$W'_{lmn} = \begin{cases} C_{lmn} + C_{mnl} + C_{nlm} + C_{nml} + C_{mln} + C_{lnm}, & \text{if } l < m < n \\ 0, & \text{otherwise} \end{cases} \quad (35)$$

The lack of ternary terms in any particular multisite-solution endmember basis does not guarantee the lack of ternary terms in any other basis. For this reason, such terms must always be considered when constructing subregular solution models.

### 3.2 Converting microscopic interactions into endmember interactions

The models presented so far are macroscopic models; they deal with the energetics of interaction between endmembers. Solution models are also frequently formulated in terms of atomic interactions [16,17,18]. Microscopic models can be described by interaction matrices of the same form and dimension as their macroscopic counterparts, with the dimensions of the interaction matrices equal to the number of site-species, rather than the number of endmembers. The elements of the matrices correspond to the site-species interactions.

There are benefits to describing the properties of a solid solution in terms of microscopic interactions. Microscopic descriptions provide a much more direct link between the physics of the interactions (for example, order-disorder, Al-Al avoidance). In addition, Powell et al. [10] argue that well-constrained values of microscopic interactions in one mineral can be used as informed guesses for other minerals. For example, Fe-Mg exchange interaction has a value of around 5 kJ per mole of sites in many silicate minerals. This concept, termed micro- $\phi$  [10], may be useful for constructing complex models where there is insufficient data to fully constrain all interactions.

Despite the benefits of parameterising solutions using microscopic models, it is usually more practical to convert these to macroscopic models [19]. Macroscopic models require fewer parameters, automatically maintain charge balance, and the set of independent endmembers can be chosen to enable more efficient computations. The linear relationship between site-species proportions and endmember proportions (Equation 5) has exactly the same form as the relationship between sets of independent endmembers (Equation 9). Therefore, the conversion from a microscopic to a macroscopic formalism is simply another form of basis conversion, allowing the mathematics of Section 3.1 to be used to convert from site interactions to endmember interactions. The untransformed endmember proportions  $\mathbf{p}$  in Equation 9 are set equal to the site-species proportions  $\mathbf{x}$ , and the matrix  $\mathbf{A} = \mathbf{E}^{indT}$ . The endmember energies  $\mathbf{G}^{mbr}$  and (macroscopic) interaction matrices calculated using the asymmetric formalism equations of Section 3.1.1 should be normalised to one mole of endmembers by multiplying them by  $n_{sites}$ . The subregular equations require only that the  $1_i W_{jk}^B$  term in Equation 28 be divided by  $n_{sites}$ .

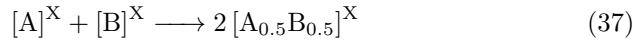
The following section describes how to populate the microscopic interaction matrices.

### 3.2.1 Binary interaction parameters

The symmetric, asymmetric and subregular formalisms all involve parameters describing the interactions between pairs of site-species. Two types of interactions are considered: simple mixing on a single site (e.g.  $\text{Mg}^{2+}$  and  $\text{Al}^{3+}$  on Site X), and two-site combinations of species (e.g.  $\text{Mg}^{2+}$  on Site X and  $\text{Ca}^{2+}$  on Site Y). Each entry in the binary interaction matrix corresponds to an energy of formation of a cluster of sites from their constituents:



For single-site mixing, the reaction can be rewritten as



Two-site (XY) energies ( $\epsilon_{[\text{A}]^{\text{X}}[\text{C}]^{\text{Y}}}$ ) cannot be obtained from experimental analyses. Instead, the energies corresponding to cross-site reactions can be used to populate the matrix. For example, the reaction



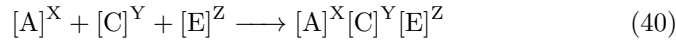
is associated with the cross-site interaction energy  $w_{ACBD,XY}$ , which is a function of the two-site energies (e.g.  $\epsilon_{[\text{A}]^{\text{X}}[\text{C}]^{\text{Y}}}$ , abbreviated as  $\epsilon_{AC}$ ):

$$w_{ACBD,XY} = (\epsilon_{BC} + \epsilon_{AD}) - (\epsilon_{AC} + \epsilon_{BD}) \quad (39)$$

In each XY block of the microscopic interaction matrix, one component can be set to zero. For the example above, let us arbitrarily choose that element to be  $[\text{B}]^{\text{X}}[\text{D}]^{\text{Y}}$ . All the remaining elements (such as  $[\text{A}]^{\text{X}}[\text{C}]^{\text{Y}}$ ) of that block are filled with values corresponding to reaction with the excluded component  $-w_{ACBD,XY}$ . Note that interaction energies involving repeated site-species (e.g.  $w_{BCBD,XY}$  and  $w_{ADBD,XY}$ ) are also set equal to zero, because the corresponding reactions have the same products and reactants [19]. A fully-worked example corresponding to that discussed in Powell et al. [10] is provided in a python package accompanying this paper (see Appendix).

### 3.2.2 Ternary interactions

The subregular model has ternary interaction parameters in addition to binary parameters. To construct a microscopic ternary matrix  $\mathbf{w}^T$ , we consider each component of the matrix to correspond to the energy of formation of a cluster of sites  $\epsilon_{[\text{A}]^{\text{X}}[\text{C}]^{\text{Y}}[\text{E}]^{\text{Z}}}$  from their constituents:



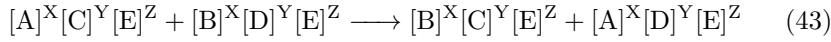
Mixing of species on the same site can be rewritten:



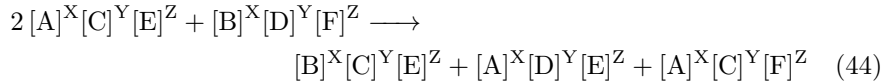
When mixing three site-species on two distinct sites, we have



The energy of formation of two- and three-site complexes includes site-bonding terms which cannot be uniquely determined by experimental means. Similar to the case of binary two-site exchange, we can arbitrarily select a single ‘‘special’’ component in each XXY or XYZ block of the ternary matrix to be equal to zero (e.g.  $[A]^X[C]^Y[E]^Z$ ), and populate the other components in that block using reactions involving the special component. Components are also set to zero if all but one of the corresponding site-species is the same as for the special component. Components sharing a single site-species with the special component are assigned values based on exchange reactions involving four clusters. For example, the component corresponding to the  $[B]^X[D]^Y[E]^Z$  cluster is assigned the negative of the following reaction energy:



Finally, components sharing no site-species with the special component are assigned values based on exchange reactions involving five clusters:



The number of non-zero (and independent) components in the XYZ blocks of the ternary matrix is therefore  $mno - m - n - o + 2$ , where  $m$ ,  $n$  and  $o$  are the number of potential site-species on the X, Y and Z sites. The XXY blocks have fewer independent endmembers (because  $[A_{0.5}B_{0.5}]^X[E]^Y$  is the same as  $[B_{0.5}A_{0.5}]^X[E]^Y$ ), but are otherwise constructed in the same way.

## 4 Discussion

### 4.1 Applications of polytope-related algebra for solid solutions

In describing the site-occupancy space of solid solutions as a polytope, we can use a variety of mathematical tools to solve various thermodynamic tasks. In this manuscript, we have discussed how to find the polytope corresponding to a solution, how to find the number of independent endmembers corresponding to the solution, and enumerating the total set of endmembers. From this starting point, other tasks are also made easier, including:

- Gridding of site-occupancy space as a function of site occupancies or end-member proportions. This is necessary for software tools such as PerpleX [20].

- Finding the independent endmember-bounded simplex within site-occupancy space which is most appropriate for a given mineral composition. This is particularly important in the fitting of thermodynamic models to experimental data. Commonly, phases in experimental runs are poor in one or more components, and therefore provide poor or misleading constraints on certain endmember reactions. In such cases, endmember basis transformation (the subject of Section 3) may provide a better set of endmembers from which to construct an endmember reaction matrix.

## 4.2 Applications for the microscopic formulation

The practise of constraining macroscopic (endmember-based) solution models from microscopic interaction parameters has already been advocated by Powell et al. [10], but there are additional benefits which are highlighted by our work.

Firstly, if the microscopic interactions  $w_{ij}$  between similar species are taken to be equal to each other (e.g.  $w(\text{AlMg}, \text{Y1}) = w(\text{AlMg}, \text{Y2})$  and  $w(\text{MgSiAlAl}, \text{Y1Y2}) = w(\text{SiMgAlAl}, \text{Y1Y2})$  for the two-site majorite solution given in Table 4), the relative endmember energies derived from the conversion described in Section 3 guarantee globally convergent ordering. In other words, the system is guaranteed to become completely disordered at a composition-dependent critical temperature. This is true regardless of the number or multiplicity of sites, and therefore provides a useful guide for model parameterisation.

Using the microscopic formulation also allows the user to continue subdividing sites to an arbitrary level without necessarily increasing the number of independent parameters. This site-splitting provides a straightforward way to reproduce observations of ordering at intermediate compositions. This could be particularly powerful in systems such as pyrope-majorite, which shows some tendency for ordering at the 50:50 composition at temperatures  $<1473$  K [3]. A small number of microscopic interactions could be used to produce models with large numbers of sites, consistently dealing with the high degree of parameter degeneracy.

Site-splitting coupled with the use of higher-order interaction parameters also presents an alternative to the use of asymmetric parameters such as  $\alpha_i \neq 1$  in the asymmetric formalism [13], or  $W_{ij} \neq W_{ji}$  in the subregular formalism [14]. These model choices have no microscopic justification, and as such may not extrapolate well. It has long been acknowledged that ordering is an important cause of asymmetry in solid solution properties [21], so site-splitting could better mirror atomic-scale processes within the same model formalism. In a similar vein, site-splitting could be used in place of “fake”-site multiplicities, where the multiplicity of one or more sites is reduced to simulate short-range ordering [22, 23]. This would produce more realistic configurational entropies when strongly-ordered species exist only in dilute quantities on a site.

**Acknowledgements** R.M. is grateful to George Helffrich and Eleanor Green for encouragement and insightful discussions.

## A Research Data

Python implementations of the polytope algorithms described in this paper are provided as [zip files attached to this draft \(during revision, online repositories with dois will be used\)](#).

Up-to date implementations can be downloaded from <https://github.com/bobmyhill/burnman/tree/polytope>, provided as a branch of the open-source *burnman* software [24].

Examples of solution model polytope generation, endmember enumeration, independent endmember (basis set) generation and gridding of site occupancy space can be found in the example script `example_solution_creation_and_manipulation.py`.

A separate code implementing the endmember and microscopic-macroscopic basis conversions for the subregular and asymmetric formalisms [14,15,10] can be downloaded from <https://github.com/bobmyhill/microphi>. A set of illustrative examples are provided.

## References

1. H.A. Bethe, Proceedings of the Royal Society of London. Series A-Mathematical and Physical Sciences **150**(871), 552 (1935)
2. G. Inden, W. Pitsch, P. Haasen, in *Phase transformations in materials* (Wiley-VCH Weinheim, 2001), p. 519
3. V.L. Vinograd, B. Winkler, A. Putnis, H. Kroll, V. Milman, J.D. Gale, O.B. Fabrichnaya, *Molecular Simulation* **32**(2), 85 (2006). DOI 10.1080/08927020500501599
4. T. Holland, R. Powell, *American Mineralogist* **81**, 1413 (1996). DOI 10.2138/am-1996-11-1214
5. T.J.B. Holland, R. Powell, *Journal of Metamorphic Geology* **24**(9), 851 (2006). DOI 10.1111/j.1525-1314.2006.00672.x. URL <http://dx.doi.org/10.1111/j.1525-1314.2006.00672.x>
6. R.O. Sack, *Petrology* **25**(5), 498 (2017). DOI 10.1134/S0869591117050071. URL <https://doi.org/10.1134/S0869591117050071>
7. T.H. Matheiss, D.S. Rubin, *Mathematics of Operations Research* **5**(2), 167 (1980). URL <http://www.jstor.org/stable/3689148>
8. D. Avis, K. Fukuda, *Discrete & Computational Geometry* **8**(3), 295 (1992). DOI 10.1007/BF02293050. URL <https://doi.org/10.1007/BF02293050>
9. J.B. Lasserre, *Discrete & Computational Geometry* **32**(1), 129 (2004). DOI 10.1007/s00454-003-0834-3. URL <https://doi.org/10.1007/s00454-003-0834-3>
10. R. Powell, R.W. White, E.C.R. Green, T.J.B. Holland, J.F.A. Diener, *Journal of Metamorphic Geology* **32**, 245 (2014). DOI 10.1111/jmg.12070
11. E. Green, R. White, J. Diener, R. Powell, T. Holland, R. Palin, *Journal of Metamorphic Geology* **34**(9), 845 (2016)
12. T.J.B. Holland, E.C.R. Green, R. Powell, *Journal of Petrology* **59**(5), 881 (2018). DOI 10.1093/petrology/egy048. URL <https://dx.doi.org/10.1093/petrology/egy048>
13. T. Holland, R. Powell, *Contributions to Mineralogy and Petrology* **145**, 492 (2003). DOI 10.1007/s00410-003-0464-z
14. G. Helffrich, B.J. Wood, *American Mineralogist* **74**(9-10), 1016 (1989)
15. J. Diener, R. Powell, R. White, T. Holland, *Journal of Metamorphic Geology* **25**(6), 631 (2007)
16. R.O. Sack, M.S. Ghiorso, *Contributions to Mineralogy and Petrology* **106**(4), 474 (1991). DOI 10.1007/BF00321989. URL <https://doi.org/10.1007/BF00321989>
17. R.O. Sack, M.S. Ghiorso, *Contributions to Mineralogy and Petrology* **116**(3), 277 (1994). DOI 10.1007/BF00306497. URL <https://doi.org/10.1007/BF00306497>
18. S. Pingfang, S. Saxena, Z. Zheru, B. Sundman, *Calphad* **18**(1), 47 (1994). DOI [https://doi.org/10.1016/0364-5916\(94\)90007-8](https://doi.org/10.1016/0364-5916(94)90007-8). URL <http://www.sciencedirect.com/science/article/pii/0364591694900078>
19. R. Powell, T. Holland, *American Mineralogist* **78**(11-12), 1174 (1993). URL <http://ammin.geoscienceworld.org/content/78/11-12/1174.short>
20. J.A.D. Connolly, *Geochemistry, Geophysics, Geosystems* **10**, Q10014 (2009). DOI 10.1029/2009GC002540

21. R.C. Newton, B.J. Wood, *American Mineralogist* **65**(7-8), 733 (1980)
22. L. Stixrude, C. Lithgow-Bertelloni, *Geophysical Journal International* **184**, 1180 (2011). DOI 10.1111/j.1365-246X.2010.04890.x
23. E.S. Jennings, T.J.B. Holland, *Journal of Petrology* **56**, 869 (2015). DOI 10.1093/petrology/egv020
24. S. Cottar, T. Heister, I. Rose, C. Unterborn, *Geochemistry, Geophysics, Geosystems* **15**(4), 1164 (2014). DOI 10.1002/2013GC005122. URL <http://dx.doi.org/10.1002/2013GC005122>